UNIVERSITY of CALIFORNIA

SANTA CRUZ

**A TELLURIUM ABSORPTION CELL FOR HIGH PRECISION
RADIAL VELOCITY CALIBRATION**

A thesis submitted in partial satisfaction of the
requirements for the degree of

BACHELOR OF SCIENCE

in

PHYSICS

by

Carl Coker

3 June 2011

The thesis of Carl Coker is approved by:

_____   _____
Professor Steven Vogt   Adriane Steinacker
Advisor   Theses Coordinator

_____
Professor David P. Belanger
Chair, Department of Physics

Abstract

A Tellurium Absorption Cell for High Precision Radial Velocity Calibration

by

Carl Coker

This thesis presents the design of a tellurium absorption cell designed for use in high precision radial velocity (RV) calibration. It is hoped that the cell will allow higher precision using the gas cell absorption technique than is currently possible. The method of extracting RVs from stellar spectra and the error analysis involved is presented, as are ways to reduce this error. The results of testing the tellurium cell at NIST on their FTS are also given. They indicate that the tellurium cell must have tight temperature control and use about half as much tellurium as it currently does, but that with improvements it may make many more spectral lines available for wavelength calibration in a bluer region of the spectrum than that currently used by iodine cells.

Contents

List of Figures

1 Introduction

Astronomers stand on the brink of being able to detect an Earth-szied potentially habitable planet. The field of extrasolar planet finding is only about 20 years old, but has advanced significantly since the first planets outside our solar system were discovered orbiting a pulsar in 1992 (Wolszczan and Miller, 1992). The first detection of a planet around a Sun-like star was made by Mayor and Queloz (1995), who found a Jupiter-mass body around the star 51 Pegasi by measuring the radial velocity (RV) the planet produced as it tugged on 51 Peg. Their method involved the use of a spectrograph to determine the shift in the star's spectral lines caused by the planet's gravitational pull.

The usual method of determining Doppler shifts in spectra is to first disperse the object's spectrum and then superimpose a reference spectrum on it. The reference spectrum is used to establish a wavelength scale on the detector (e.g., on a CCD, the number of pixels that correspond to a given change in wavelength). The more lines that are present in the reference spectrum, the more accurately the wavelength scale can be established, due to the increase in the number of data points.

Traditionally, lamps with a known emission spectrum were used for this reference. With an error of up to $1\,\mathrm{km\,s^{-1}}$ on the calculated velocity (R. Griffin and R. Griffin, 1973), it was not very accurate. This inaccuracy came about because of the differing path lengths the light from the star and that from the reference lamp traveled, which generated large systematic errors. Because of these errors, and due to the fact that even Jupiter only produces a maximum RV on the Sun of

$\sim 10\,\mathrm{m\,s^{-1}}$, something better was clearly needed to detect planets.

This new system was finally proposed by Griffin and Griffin (1973). They suggested using telluric lines, or spectral lines due to absorption by gases in the Earth's atmosphere, and were able to improve the precision of RV measurements to $\sim 50\,\mathrm{m\,s^{-1}}$. However, due to the fact that it relied on atmospheric composition, this method fell prey to the rapid changes in the Earth's atmosphere caused by the local weather as well as high altitude winds, and it was confined to certain wavelength ranges due to the atmosphere's absorption characteristics. Koch and Wöhl (1984) were the first to use an iodine cell as a spectroscopic instrument, placing a glass ampule filled with iodine into the optical path of their solar spectrograph, superimposing the iodine sample's absorption lines on the solar spectrum. This allowed them to determine solar RVs to an accuracy of $\pm 15\,\mathrm{m\,s^{-1}}$. Marcy and Butler (1992) further describe the use of an iodine cell to measure precision RVs of other stars, for a variety of purposes. Their main objective was to detect extrasolar planets.

Further refinements to the absorption cell technique have resulted in higher precision still, but there is a limit to how far the iodine design can be pushed. This is because Iodine only has so many spectral lines, and RV precision goes approximately as $\sqrt{N_{lines}}$. An element that has a high density of lines in a different spectral band will provide a complementary highly accurate reference. One element that fits the bill is tellurium, the element next to iodine on the periodic table. It has a very high line density from $\sim 3850 - 5000\,\mathrm{\AA}$, creating the additional benefit that it covers a denser region of stellar spectra, hopefully allowing a much higher precision. This high precision would allow the detection of Earth-mass planets in Earth-like orbits.

However, even at the low pressures involved, tellurium sublimates at $\sim 550\,^{\circ}\mathrm{C}$, a far higher temperature than the $50\,^{\circ}\mathrm{C}$ that iodine cells are operated at. Because of this, the cell must be thermally isolated from the rest of the sprectrograph. Even with active cooling, the blackbody radiation emitted by the heating elements and the cell itself can create a seriously objectionable noise source if not carefully controlled. The main aim of the project was to design and build a prototype apparatus for containing the cell and heaters and then test it to see whether it could

produce usable spectra despite the problems brought on by blackbody radiation produced at its high temperature.

2 Extracting RVs From Spectra

2.1 Main Approach

When spectra are taken using a gas absorption cell for RV measurements, the gas's spectrum is superimposed on the stellar spectrum, creating many blended lines. In order to disentangle the two spectra and determine the Doppler shift present, as well as account for the instrumental effects described in Section 3.3, both they and the instrument itself must be modeled. For the instrument, this takes the form of its point-spread function, or PSF. The PSF determines what happens to the image of a point source as it travels through the instrument. Since an image essentially consists of many point sources, convolving the PSF with the spectrum gives its appearance on the CCD.

The raw spectra consists of the product of two functions convolved with the PSF: the stellar spectrum itself, I_s, and the spectrum of the gas cell (i.e., its transmission function T_g). The stellar spectrum is shifted by some amount $\Delta\lambda$, which is what is being measured. This gives an observed spectrum of

$$I_{obs}(\lambda) = k[T_g(\lambda)I_s(\lambda + \Delta\lambda)] \circledast \text{PSF} \tag{2.1}$$

(Butler et al., 1996), where k is a normalization factor and $\circledast$ represents convolution. The spectra of the star and the gas cell are multiplied together because they are acting as transmission functions instead of pure brightness measures.

Obtaining T_g is fairly simple; the cell's spectrum is just taken using a spectrometer with very high precision compared to the one being used to obtain RVs; Butler et al. (1996), as well as Marcy

and Butler (1992) used the Fourier Transform Spectrometer at Kitt Peak National Observatory, which generated spectra with a resolution of $\lambda/\Delta\lambda = 10^6$ and had a signal to noise ratio of 700 (for comparison, the Hamilton spectrograph they used for their observations had a resolution of 120,000 and a typical S/N of 250 for their targeted stars). The iodine spectra may then be compared with these atlases to establish a wavelength scale for each exposure.

Measuring I_s is harder, and obviously must be done for each individual star. Reference observations of each star are taken without the cell in place, yielding a spectrum

$$I_{o,s} = kI_s(\lambda + \Delta\lambda) \circledast \text{PSF} \qquad (2.2)$$

The spectra still need to be deconvolved from the PSF. In order to get the PSF, bright rapidly rotating B type stars are observed through the gas cell, bookended before and after the star observation (Butler et al. 1996). Since T_g is known from the reference observations performed earlier, the B star spectra can be compared to this reference, allowing the PSF to be measured as described in Section 2.2. The PSF so obtained is then used to deconvolve $I_{o,s}$ to get I_s.

At this point, the spectrum is broken up into several hundred pieces, which each contain the same number of pixels. The spectrum is then sampled at four times the sampling rate of the CCD (i.e., for every actual pixel, four model pixels are used). This is done in order to preserve any high-frequency information present in the spectrum (Butler et al., 1996). A spline is then used to fit the observed spectrum to the template taken earlier. The difference between the two is the Doppler shift.

Once the Doppler shift itself has been measured, it can be transformed into an RV using the Doppler formula:

$$\lambda = \lambda_0 \frac{(1 + \beta cos\theta)(1 + \rho_g)}{n\sqrt{1 - \beta^2}} \qquad (2.3)$$

(Marcy and Butler, 1992), where λ_0 is the rest wavelength, $\lambda = \lambda_0 + \Delta\lambda$, $\beta = v/c$, n is the refractive index of the air inside the spectrometer, ρ_g is the gravitational redshift of the starlight, and θ is the angle between the line of sight to the star and the star's velocity relative to the Earth's surface. Ordinarily, the general relativistic and refractive corrections could be ignored, since they are of order

$< 1\,\mathrm{m\,s}^{-1}$ (Marcy and Butler, 1992). However, since the reason behind building the tellurium cell is to push below that level of precision, they must be incorporated.

2.2   Determining the PSF

The method of determining the PSF given here is the same as that presented by Valenti et al. (1995). First, the spectrum of a reference source (here, the gas cell or the rapidly rotating B star) is taken through the instrument to be used. Next, this observed spectrum is compared with its known spectrum convolved with a synthetic PSF that has several free parameters. Using non-linear least squares fitting, the parameterized PSF is adjusted until it produces the best fit to spectrometer's PSF.

As mentioned in the previous subsection, an observed spectrum $f(x)$ takes the form of a convolution of the spectrum of light incident on the spectrometer, $g(\lambda)$, and the detector's PSF, $\phi(x)$:

$$f(x) = \int_{-\infty}^{\infty} g[\lambda(x')]\phi(x - x')dx' \tag{2.4}$$

Here, x refers to position along the direction of dispersion on the CCD, while $\lambda(x)$ is a function that associates each wavelength of light incident on the spectrometer with its position on the CCD. This convolution is normalized by requiring that

$$\int_{-\infty}^{\infty} \phi(x - x')dx' = 1 \tag{2.5}$$

By labeling the N pixels on the CCD with indices i running from 0 to $N-1$, and labelling the positions on either side of pixel i x_i and x_{i+1}, a discrete mathematical description of the observed spectrum can be defined:

$$f_i = \int_{x_i}^{x_{i+1}} f(x)dx \tag{2.6}$$

Similar discretizations of the intrinsic spectrum g and the PSF can be performed, resulting in a complete mathematical description of the spectrometer.

With this in hand, the synthetic PSF can be constructed and fitted to the observed one. Since most astronomical instruments are approximately Gaussian or sinc ($\mathrm{sinc}(x) = \sin(x)/x$) functions, they are usually the best place to start (Valenti et al. 1995). A careful balance of flexibility must be struck with the choice and number of free parameters; if there are too many, noise in the spectrum can produce artifacts in synthetic PSF, while if there are too few, the PSF can not be fitted accurately. The method used by both Valenti et al. (1995) and Butler et al. (1996) is to use a central Gaussian of fixed height and several satellite Gaussians whose heights form the free parameters of the fit. The height of the central Gaussian is constrained by the overall normalization of the spectrum in question. With the free parameters in hand, a non-linear least squares fit is performed on the spectra, resulting in the PSF associated with the observed spectrum.

3 Spectroscopic Error Sources

3.1 Spectral Noise Sources

3.1.1 Photon Noise

When the spectrum is taken off the CCD and analyzed, it is binned into several equal pieces, each of which contains the same number of pixels (Butler et al ., 1996). Each pixel has a Doppler measurement associated with it, $V(i)$, and some error σ_{v_i}. The mean velocity measurement taken from the piece, $\bar{v}$, also has an error

$$\sigma_{\bar{V}} = \frac{1}{\sqrt{\sum \left(\frac{1}{\sigma^2_{V(i)}} \right)}} \tag{3.1}$$

associated with it, assuming the error from each pixel to be different and uncorrelated. In the case that the error on each pixel is equal, this reduces to $\sigma_{\bar{V}} = \sigma_{V(i)}/\sqrt{N}$, where N is the number of pixels.

The error on each pixel can be obtained as follows: consider a stellar spectrum I_0 with no Doppler shift that has much lower noise than the observed, shifted stellar spectrum I. Let these spectra have identical intensities, effectively ignoring instrumental defects/effects (Bouchy et al., 2001). For small Doppler shifts such as those encountered in high precision RV work, the difference in intensity between the two spectra is given by

$$I(i) - I_0(i) = \frac{\partial I_0(i)}{\partial \lambda(i)} \Delta \lambda(i) \tag{3.2}$$

The Doppler shift for each pixel is

$$\frac{\Delta V(i)}{c} = \frac{\Delta \lambda(i)}{\lambda(i)} \tag{3.3}$$

Combining these two equations, the Doppler shift can be written as

$$\frac{\Delta V(i)}{c} = \frac{I(i) - I_0(i)}{\lambda(i)(\partial I_0(i)/\partial \lambda(i))} \tag{3.4}$$

(Bouchy et al. 2001). Thus, the Doppler shift for each individual pixel is measured by the change in intensity across it caused by that shift.

The error on each piece of the spectrum is then

$$\frac{\sigma_{V(i)}}{c} = \frac{\sigma_{I(i)}}{\lambda(i)(\partial I_0(i)/\partial \lambda(i))} \tag{3.5}$$

, as the noise on I_0 was assumed to be negligible. Substuting into Equation 3.1, then, the error across one piece of the spectrum is

$$\sigma_{\bar{V}} = \frac{1}{\sqrt{\sum \left(\frac{\sigma_{I(i)}}{\lambda(i)(\partial I_0(i)/\partial \lambda(i))}\right)^2}} \tag{3.6}$$

This is the photon-limited Doppler error in velocity measurements taken from any piece of the spectrum, and it can be extended to cover the entirety of the spectrum easily. It can also be represented by a quality factor, Q, given by

$$Q = \frac{\sqrt{\sum \left(\frac{\sigma_{I(i)}}{\lambda(i)(\partial I_0(i)/\partial \lambda(i))}\right)^2}}{\sqrt{\sum I_0(i)}} \tag{3.7}$$

(Bouchy et al., 2001). This turns the error on the spectrum into

$$\sigma_{\bar{V}} = \frac{1}{Q\sqrt{\sum I_0(i)}} \tag{3.8}$$

The advantage of this formulation is that Q is independent of the intensity. It solely represents the quality and richness of the spectrum (Bouchy et al., 2001). The more line rich the stellar spectrum is, the higher the quality factor, and the lower the error. Note that $\sum I_0(i) = N_{e^-}$ is simply the number of electrons liberated from the CCD by the incoming light, so that finally

$$\sigma_{\bar{V}} = \frac{1}{Q\sqrt{N_{e^-}}} \tag{3.9}$$

3.1.2 Wavelength Calibration

In order to calibrate the wavelength scale of each observed spectrum, the reference lines (be they iodine, tellurium, or ThAr) in that spectrum are compared and fitted to a spectral atlas whose precision is much greater than that of the spectrometer used to observe the target (Butler et al., 1996). By fitting the spectra to each other, the wavelength zero point of the observed spectrum can be set, and Doppler measurements can then be extracted. Since the calibration fitting is done using the same method as that for extracting the Doppler data as described in Section 1.1, the analysis in the preceding section applies here as well.

3.1.3 Reducing Photon Noise and Wavelength Errors

The two largest sources of error in high-precision RVs are photon noise and wavelength calibration errors, since the stellar noise is counteracted by carefully chosen observing strategies (see Section 3.3.1), and imperfections in the instrument are either small or corrected by modelling the PSF for each exposure (Section 3.2). There are two main ways to decrease these remaining errors: use longer integration times/more data points, and increase the number of lines used during wavelength calibration and scaling. Taking more data will work well, but it is infeasible due to the limited availability of telescope time, as well as a need to observe as many stars as possible.

Therefore, the best strategy for improving spectroscopic precision, assuming the spectral atlases used as a basis for comparison are far more accurate than the spectra being taken at the telescope, is to increase the number of lines used to measure RVs, in both the stellar and gas reference spectra. As in Section 3.1.1, consider a spectrum that is binned into many equal pieces; let each piece contain one spectral line. As before, $\sigma_{V(i)}$ is the error associated with the velocity measurement from each piece, except here it also is the error for each individual spectral line. Following the same analysis, the mean error will be

$$\sigma_{\bar{V}} = \frac{1}{\sqrt{\sum \frac{1}{\sigma_{V(i)}^2}}} \tag{3.10}$$

Assuming the errors on each line are all approximately the same, then $\sigma_{\bar{V}} \approx \sigma_V/\sqrt{N}$, where N is the number of lines used in the measurement.

In the case of the stellar spectrum, Q increases as more lines are added. This is because of the $\partial I_0(i)/\partial \lambda(i)$ term. As N increases, the contribution from that term does as well, as the intensity changes more rapidly over a given pixel. For example, assume that each spectral line is roughly identical in depth and width. Then, doubling the number of lines will also double the contribution from that term and increase Q by a factor of $\sqrt{2}$. This means that the photon noise error present in the stellar spectrum also goes as $1/\sqrt{N}$. Therefore, increasing the number of lines available in both the stellar and reference spectra improves the precision to which RVs can be measured.

3.2 Instrumental Effects

3.2.1 PSF Asymmetries

The PSF is asymmetric due to manufacturing imperfections in the optics, imperfect alignment, dust and other contaminants present on all surfaces, seeing effects due to possible air currents in the spectrometer and telescope rooms, etc. These imperfections shift the PSF from a pure Gaussian and thereby cause shifts in the observed spectral lines which are not due to Doppler effects, but will still be accounted for as such unless the PSF is modeled and deconvolved from each spectrum.

In order to estimate the error induced by this effect, consider an asymmetry in the PSF that shifts a spectral line by some amount δ (Butler et al., 1996). If the line is narrow, it will be shifted by almost exactly δ, since the PSF is essentially being convolved with a delta function. A broader line will not behave this way, and thus will not shift by δ, meaning that the PSF displaces each line by a different amount, introducing a potentially large error. Since the stellar lines are broader than the relatively narrow reference lines, there will be a systematic shift between the two (Butler et al., 1996).

In order to calculate the shift, the PSF must be calculated for each exposure. Since the PSF also changes over the surface of the CCD, it must be calculated for each piece of the spectrum as well. In the iodine referenced spectra taken by Butler et al. (1996), about 100 different iodine lines were typically used to measure the PSF to within $\sim 0.5\%$, which translated to a systematic error of $\sim 2\,\mathrm{m\,s^{-1}}$.

3.2.2   CCD Imperfections

No CCD is perfect, and each pixel is not a perfectly square, uniform potential well. Each pixel is not the same size as its neighbors, nor are they spaced perfectly evenly. Because of this, as spectral lines move across the pixel boundaries, Doppler error will be incurred. When averaging over the entire CCD, the inhomogeneities tend to disappear, meaning that the error induced by them is not purely systematic in nature (Butler et al., 1996). Therefore, they are characterized as a random error that is some percentage of the dispersion of the spectrometer (given in $\mathrm{m\,s^{-1}}$/pixel). Fully characterizing this error is difficult at best, however. Even so, Lovis et al. (2006) performed several tests on the CCD used with HARPS, determining that these errors remain well below the precision limit imposed by photon noise and wavelength calibration.

Another effect caused by the CCD is charge transfer inefficiency, or CTI. Not all of the electrons released from each pixel are able to move over the adjacent pixels and reach the signal register which records the data. This inefficiency is quantified as the fraction of charge that successfully transits adjacent pixels. The effect manifests itself as a decrease in the illumination of pixels farther from the register, which can produce spurious Doppler shifts. It tends to get smaller as signal to noise ratio increases, and is a non-factor at the very high S/N's used by the gas cell technique when the precision required does not exceed $1\,\mathrm{m\,s^{-1}}$ (Bouchy et al., 2009). However, because the tellurium cell is aimed at going far below this threshold, modelling it may be necessary. Fortunately, it may be calibrated and measured using the same ThAr lamps as are used in the initial calibration steps performed for each night of observing, following the method outlined by Bouchy, et al. (2009).

3.3   Astrophysical Noise Sources

3.3.1   Stellar Noise

There are three main types of stellar noise: p-mode oscillations, granulation, and jitter related to stellar activity (Pepe and Lovis, 2008; Lovis et al., 2006). P-mode oscillations are acoustic vibrations on stellar surfaces due to density fluctuations within the star, and generally have periods on the order of a few minutes. They tend to produce velocity shifts of up to several $\mathrm{m\,s^{-1}}$, but are also the easiest stellar noise source to eliminate. Simply observing over a time period 2-3 times longer than the oscillation period tends to almost completely average them out, leaving the residual error at only a few $\mathrm{cm\,s^{-1}}$ (Pepe and Lovis, 2008; Dumusque et al., 2011).

Granulation is due to convection in the star's atmosphere. A star's photsphere consists of many convection cells, and the motion of hot gas towards the surface and cooler gas below in these cells can also induce velocity shifts of several $\mathrm{m\,s^{-1}}$ (Pepe and Lovis, 2008). The periods associated with granulation are much longer (anywhere from 30 minutes to 30 hours) than for p-mode oscillations, so the strategy of simply taking exposures of longer duration than the noise-source period is infeasible. Instead, later-type, quieter stars such as the yellower G and K type stars are observed, taking care to avoid any stars with high activity within that range as well. Another strategy that can be employed is to take multiple observations of a target star per night, each separated by a few hours; this reduces the error somewhat more than taking longer observations (Dumusque et al., 2011).

Stellar activity-induced jitter is the velocity shift due to activity on the star's surface such as sunspots and other magnetic phenomena. As shown by Dumusque, et al. (2011), sunspot activity can cause a Doppler shift at the $\mathrm{m\,s^{-1}}$ level by causing differences in flux between the redshifted and blueshifted portions of the star. The more and larger sunspots exist on the star's surface, the more noise there will be. The period of this noise is determined by the star's rotation rate; because stars are not rigid bodies and thus different latitudes rotate at different rates, there will be

several periodicities in the sunspot noise signature laid on top of each other (Dumusque et al., 2011). For most Sun-like stars, the periods will be clustered around a time of 20-30 days. One potential strategy for reducing spot noise is to observe the star every two or three nights, depending on the star's rotational period; by combining this with the strategies for reducing granulation and p-mode noise, the effect of all three stellar noise sources can be brought down to below about $10\,\mathrm{cm\,s^{-1}}$ (Dumusque, et al. 2011).

3.3.2   Barycentric Corrections

Because the precision which we are striving to attain is so high, we must correct for the motion of Earth around the Sun, as well as for general relativistic effects. These factors include: time dilation, gravitational blueshift due to the gravitational fields of both Earth and the Sun, change in stellar coordinates due to its own motion, and the apparent acceleration due to the star's transverse velocity. In order to measure these, the flux-weighted midpoint of each observation is recorded, with the necessary accuracy being about 10 seconds or less (Butler et al., 1996). With that accuracy, these corrections are precise to within $0.1\,\mathrm{m\,s^{-1}}$ (Butler et al., 1996).

4 Cell Design

4.1 Why Tellurium?

As mentioned in Section 1, a tellurium absorption cell must be operated at temperatures exceeding $500\,^{\circ}\mathrm{C}$ to provide stable, consistent spectra. This makes the design inherently more difficult to work with, much worse than alternatives such as the iodine cells currently in use or the fiber optic piped emission lamps used by instruments such as HARPS and the ELODIE spectrograph. However, tellurium offers several advantages that these alternatives do not. As shown in Fig. 4.1, spectra of G, K, and M stars, the main targets of planetary surveys, exhibit increased line density toward the bluer regions of the spectrum, particularly the B band (Bouchy et al., 2001). Tellurium's useful wavelength range is $\sim 3850 - 5000\,\text{Å}$, covering almost the entire B band and about half of the V band, making it ideal for catching the increased line density that the target stars exhibit there. Iodine's useful range by contrast is about $5000 - 6000\,\text{Å}$, and thorium argon (ThAr) lamps like those used by the HARPS team tend to have a useful range spanning $\sim 3800 - 6900\,\text{Å}$, covering almost the entirety of the visual spectrum (Lovis et al., 2007).

Tellurium is additionally the only known source which provides a line density comparable to or better than that of Iodine. While the ThAr lamps only have about 8400 useful lines in their entire range (Lovis et al., 2007), Iodine cells have several available features per angstrom (Butler and Marcy, 1992), and as seen in Fig. 4.2, the tellurium spectrum shows a similar if not greater density. Tellurium also has the advantage that there are virtually no telluric lines in its useful range,
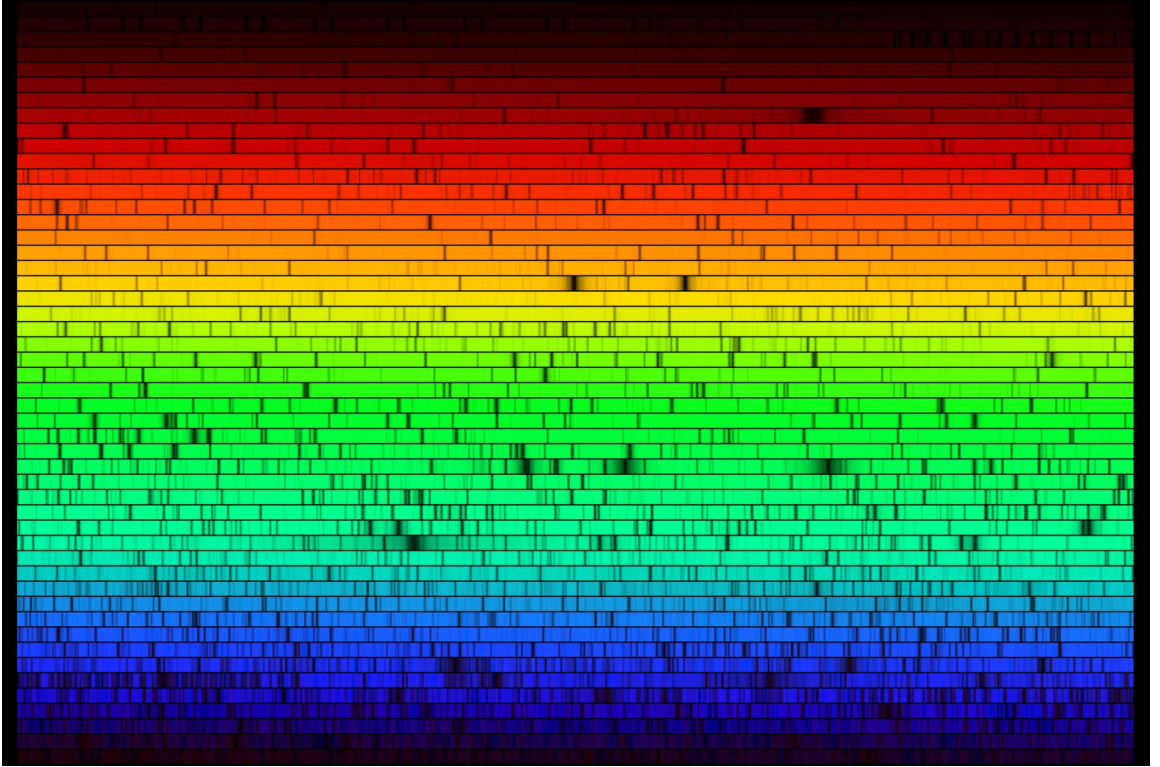
Figure 4.1: The solar spectrum (spectral type G2), taken across the visual range of 4000 to 7000 Å and presented here as a point of comparison against the main target stars (G, K, and M class). The line density shows a marked increase in the bluer regions as compared to the red, with many strong features between 5000 and 4000 Å, the region where tellurium has its highest line densities.

Source: N.A.Sharp, NOAO/NSO/Kitt Peak FTS/AURA/NSF, http://www.noao.edu/image_gallery/html/im0600.html

while there are many redward of 6000 Å; these lines add noise and are difficult to average over.

Using tellurium also enables us to take advantage of the benefits of a gas absorption cell. Because they require no modification of the sprectrometer itself, they can be easily retrofitted onto existing instruments if there is available space. They are also relatively cheap. The fiber fed emission lamp approach requires building entirely new instruments such as HARPS, and the optics of these instruments must be scaled up along with the telescope they are used with (Cochran et al., 2008).

One potential concern about tellurium is thermal Doppler broadening of its spectral line due to its high temperature. The lines are Doppler broadened by an amount

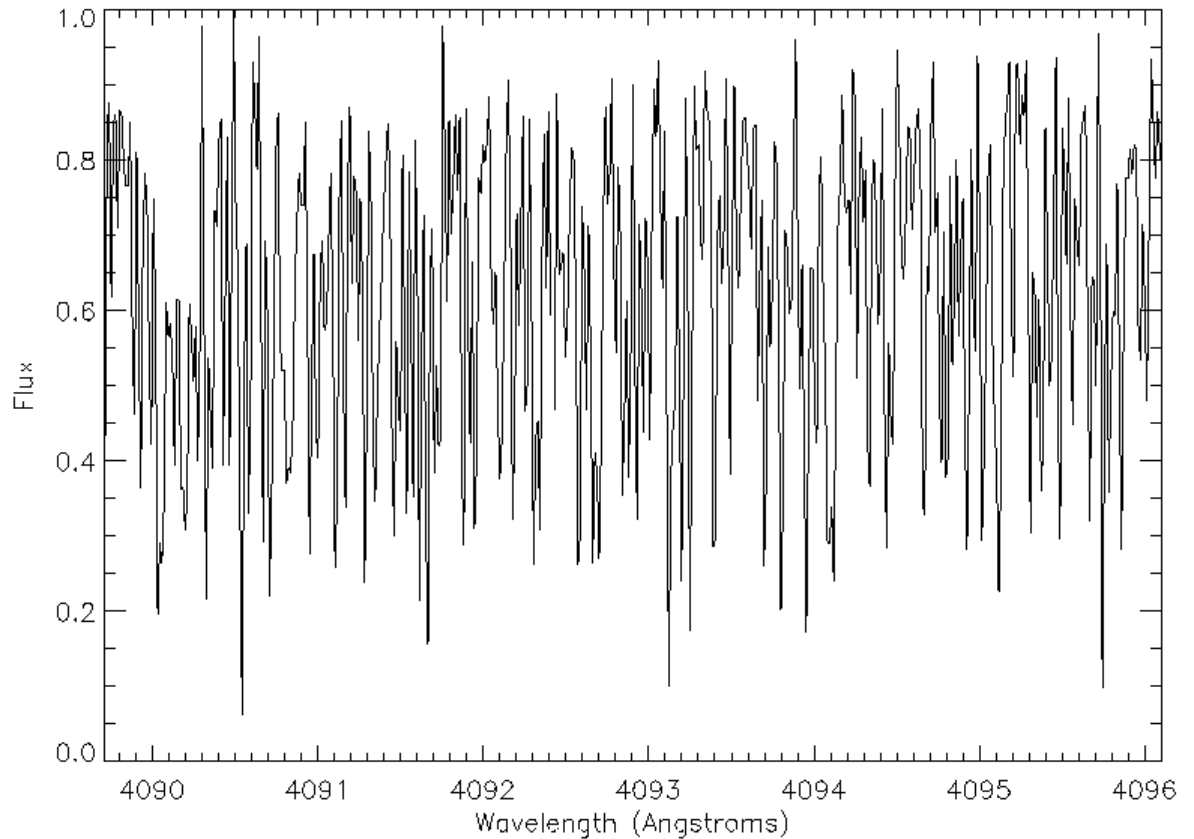$$\Delta\lambda = \sqrt{\frac{8kT\ln 2}{mc^2}}\lambda_0 \tag{4.1}$$

Figure 4.2: A six angstrom wide section of the tellurium spectrum. The spectrum has been continuum normalized (see Section 5 for details), and the resolution is $\lambda/\Delta\lambda \approx 400,000$, where $\Delta\lambda$ is the width of the smallest feature that can be measured. Note the high density of lines, with several potentially usable features per angstrom.

(Foot, 2005). Here, k is the Boltzmann constant, T the temperature of the gas, m the mass of the atom, and λ_0 the initial line wavelength. For the strong line at 4095.75 Å, this translates to a widening of ~ 0.005 Å. Given the line's apparent approximate width of 0.02 Å, this represents a significant effect. However, in an iodine cell, with a similar weight molecule and a temperature of ~ 325 K, as well as similar line widths, the Doppler broadening is of a similar magnitude; an iodine line at 5000 Å would be be broadened by 0.004 Å, indicating that Doppler broadening in tellurium will not significantly effect the accuracy of the spectrum.

4.2   Design Challenges and Solutions

First and foremost, the cell is operated at a very high temperature. Because of this, it must be thermally isolated from the rest of the spectrograph as much as possible. The best way to do so is to block heat transfer due to conduction or convection by mounting the cell on very thin guy-wires inside a vacuum dewar. However, the radiant heat output of 100 W (see Appendix A) will still be transferred to the dewar, meaning that it must be cooled. Two methods were considered: copper piping attached to the outside of the dewar, and a water jacket. Although the water jacket was more work to incorporate, it was decided that it would be too difficult to maintain good contact between the pipes and the dewar; loss of contact would severely restrict heat transfer between the dewar and the pipes, rendering them useless as a cooling solution. The water in the jacket must be cycled to keep the dewar cool; to this end, it is connected to a chiller mounted outside the spectrometer.

Preliminary testing in air using a fused silica tube in place of the actual tellurium cell revealed that the cell will act as a lightpipe while having very little visual blackbody emission as compared to the heaters (see Fig. 4.3). Therefore, the heater's glow will be visible to the instrument even though it will be looking straight down the cell. To combat this, a layer of opaque silver foil has been placed between the heaters and the cell. The silver's low emissivity helps restrict its blackbody radiation in the visible range, lessening the lightpipe effect. Reflective baffles have also been put in place to block the glow of the heaters themselves.

However, this still leaves the infrared radiation, which fused silica is very transparent to (Drummond, 1936). Happily, hot mirror coatings are commonly available which block infrared light while passing the visible spectrum; however, they were not implemented for this first prototype. The fused silica windows were chosen for their high transparency and high bakeout, or maximum operating, temperature of 400 °C.

Lastly come the comparatively minor problems of both heating the cell and powering the heaters. To heat the cell, band heaters using nichrome wire as the heating element with mineral insulation are employed. Two heaters are required due to the nub in the middle of the cell. The
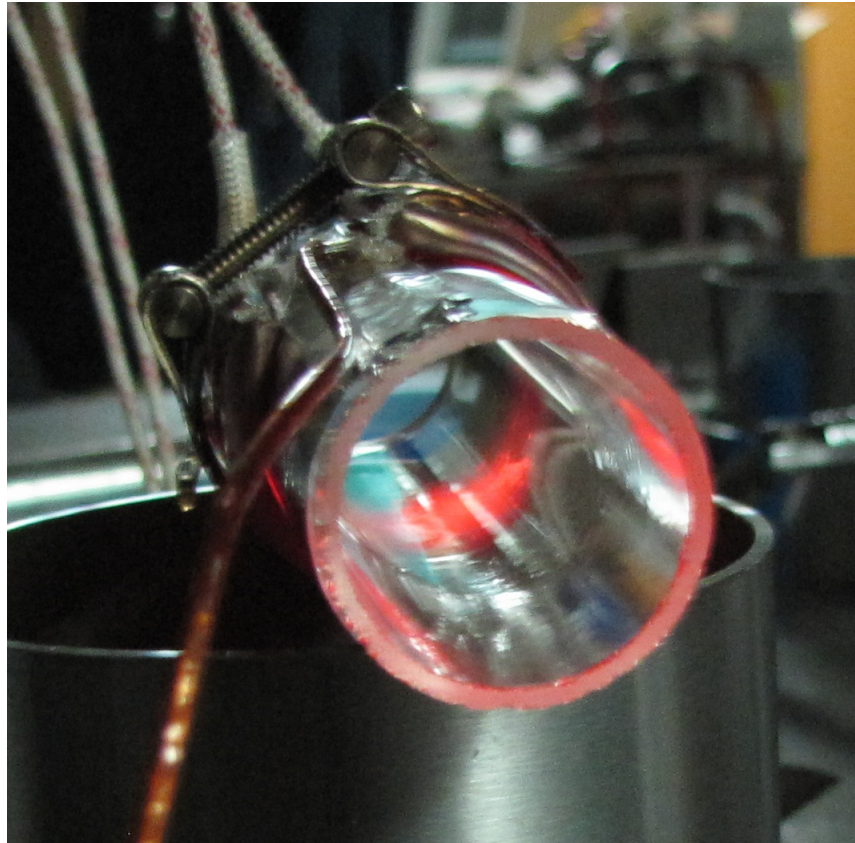
Figure 4.3: Testing apparatus using the fused silica tube in place of the cell. The heaters glow quite strongly, and the light from the inner surface of the heaters is piped by the silica to the end of the tube.

Image credit: Terry Pfister, engineer at UCO/Lick.

heaters are powered by leads strung through specially constructed conduits in the side of the dewar.

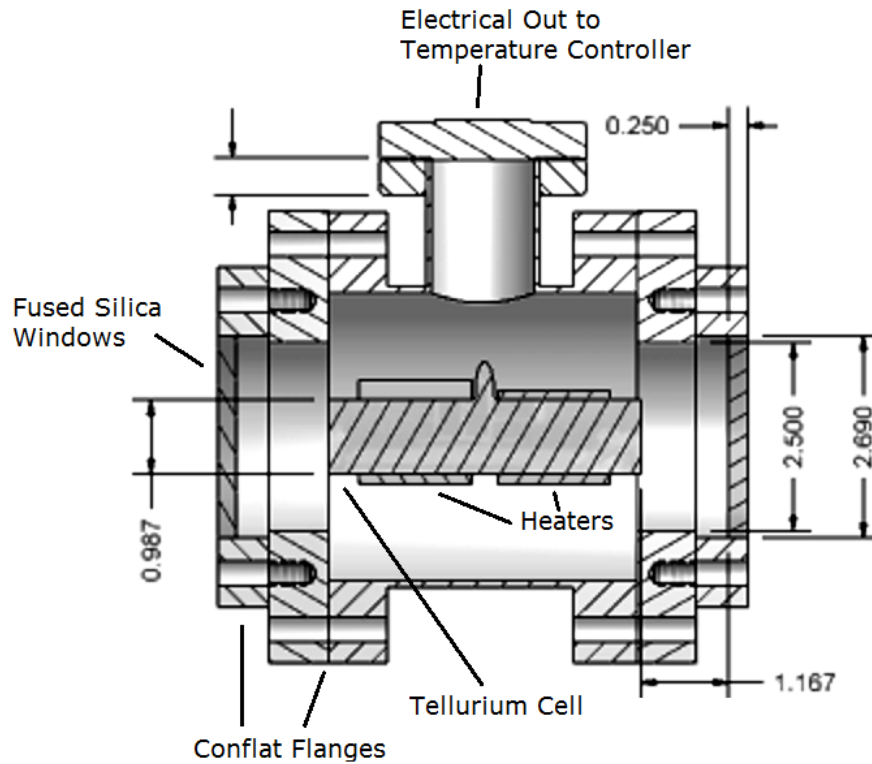For a complete diagram of the cell assembly and dewar, see Fig. 4.4.

Figure 4.4: A diagram of the tellurium cell apparatus. The cell is covered with silver foil and the band heaters are clamped around it. Guy-wires suspend the cell in place. The dewar windows are held in place using Conflat knife-edge vacuum flanges, which are sealed against the dewar wall using copper O-rings. The heaters' temperature is monitored using internal Type J thermocouples, and they are controlled using an Omega temperature controller. The water jacket consists of copper ribbon tubing that is clamped to the outside of the dewar, and is shown in the next figure. Measurements are in inches.

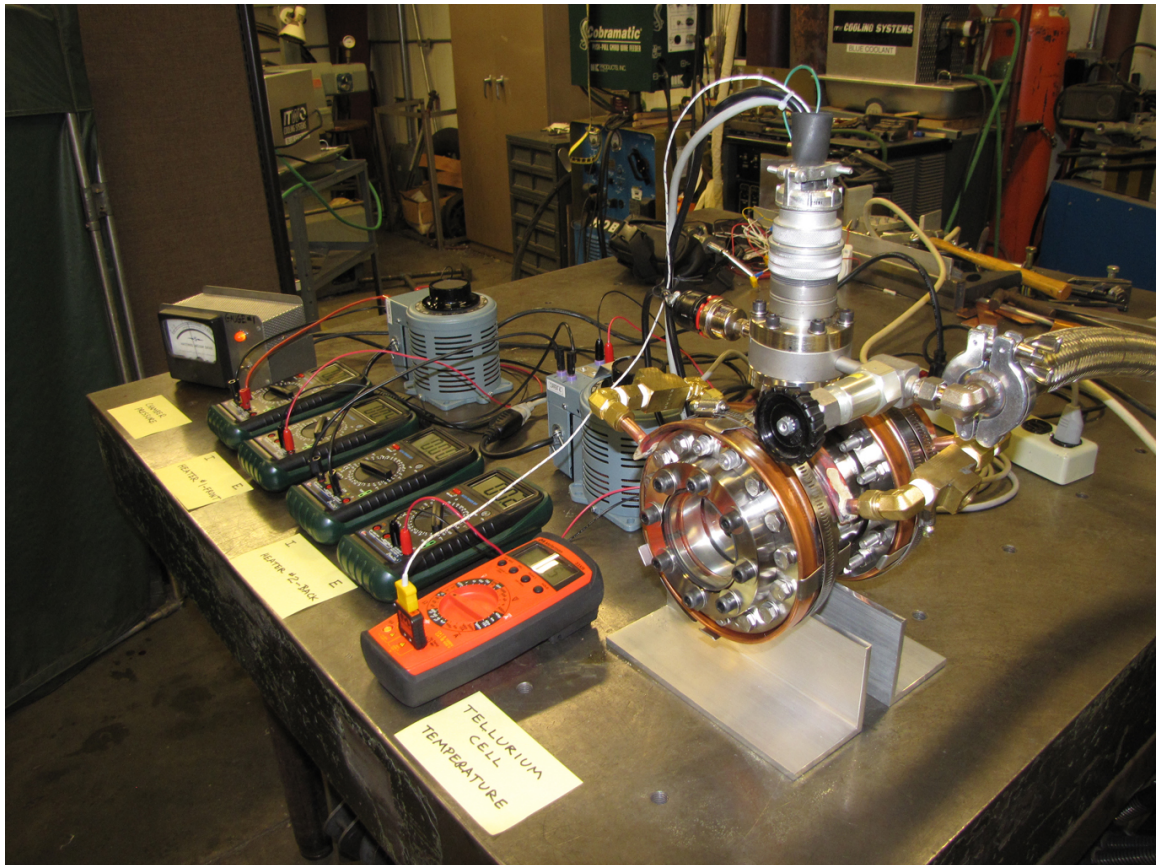Image credit: Terry Pfister, engineer at UCO/Lick.

Figure 4.5: The tellurium cell fully assembled in the Lick shops before being sent to NIST for testing. The multimeters are for monitoring the temperatures of each component inside the dewar, and the water jacket can be seen clamped around the outside of the cell.

Image credit: Prof. Steven Vogt, UCO/Lick.

5 NIST Testing and Results

The cell was transported to the National Institue of Standards and Technology (NIST) for testing on their Fourier Transform Spectrometer (FTS). The purpose of this testing was to determine the usable range of the tellurium cell (i.e., the region in which the line depth is large enough for good precision to be achieved on RV data), as well as to determine if the cell's thermal radiation would render the spectra unusable. The NIST FTS uses a xenon emission lamp as the illumination source, meaning that xenon emission lines are present in the raw test spectra. Five spectra of the cell were taken before it failed on the sixth run. On that sixth run, the cell became too hot, and the surface of the aluminum bar holding the cell evaporated, coating the cell windows.

The fourth and fifth runs provided the most useful spectra, using a hot mirror and two different types of blue filter (a BG14 for the fourth, and a Corning 5-56 for the fifth). Flat field exposures were taken of the xenon lamp with both of these filter combinations so that its emission lines could be removed from the spectra. After they were divided away, the spectra were continuum normalized by fitting a cubic spline to the remaining slope present in the continuum (i.e., the base light curve on which the tellurium lines were superimposed) and dividing that away. The now flattened spectra were then normalized to 1.0, to provide the line depths at a glance. The full continuum normalized spectra containing the Tellurium region are shown in Figs. 5.1 and 5.2.

The cell temperature during the fourth run held at $581\,^{\circ}\text{C}$, while during the fifth it was allowed to rise. It never got hotter than $593\,^{\circ}\text{C}$, as either at that point or a little cooler, the surface of the aluminum bar inside evaporated, as described above. The spectral lines are deeper in the
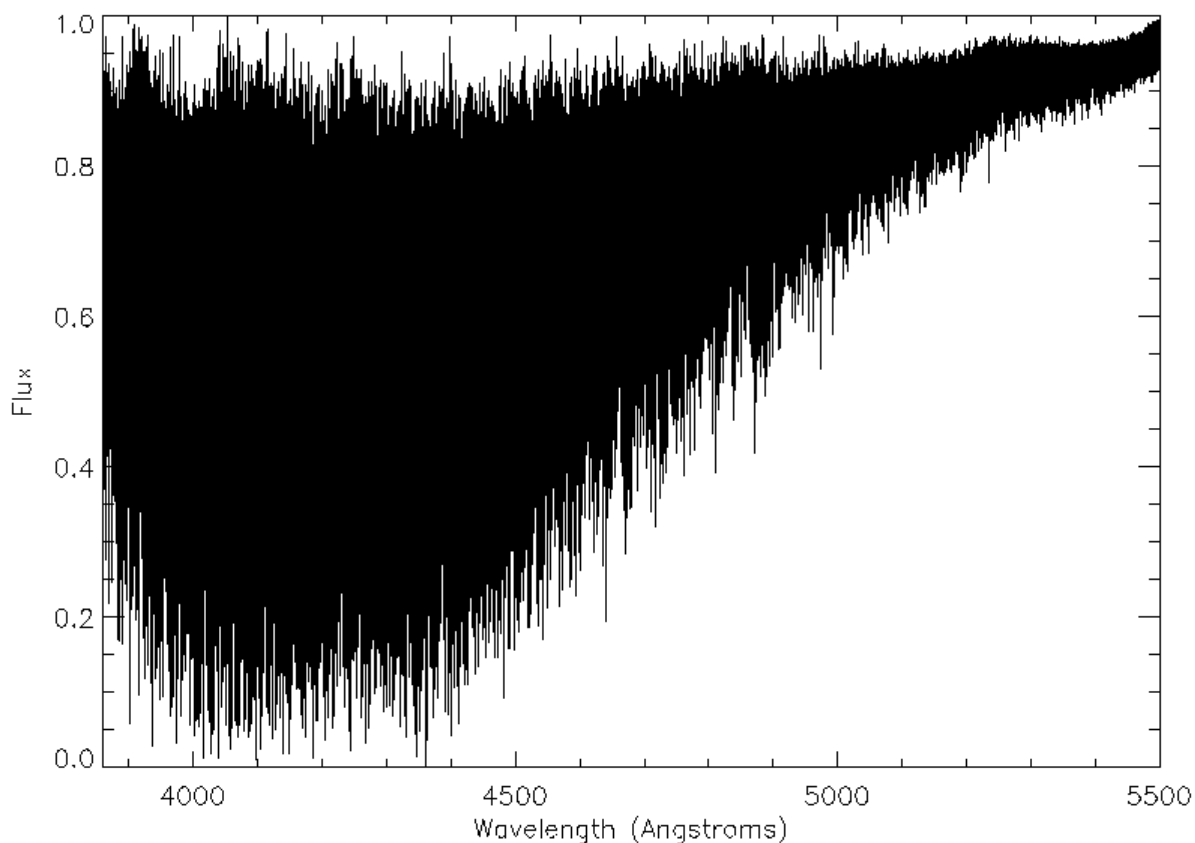
Figure 5.1: The continuum normalized spectrum of the tellurium cell from the fourth run, at a temperature of 581 °C.

fifth run (as shown in Fig. 5.3), indicating that higher temperatures cause the lines to deepen. This effect means that the temperature of the cell will have to be maintained quite closely, as changing line depths would introduce systematic error into the wavelength calibration.

Fig. 4.2 shows a small section of the fourth run, to better show the density of the spectrum. Based on a rough measurement of the full width at half maximum (FWHM) of the line at 4095.75 Å seen in Fig. 4.2, the resolution of these scans ($R = \lambda/\Delta\lambda \approx \lambda/\text{FWHM}$) is $\sim 400,000$. A boxcar smoother was applied to the spectrum in Fig. 4.2 to simulate how the spectrum would appear at a typical planet-hunting resolution of $\sim 80,000$; the result is shown in Fig. 5.4. In that smoothed section of the spectrum, there is an average of 5-7 usable features per angstrom. Assuming that average holds across the entirety of the tellurium absorption band (width ~ 1200 Å), there are
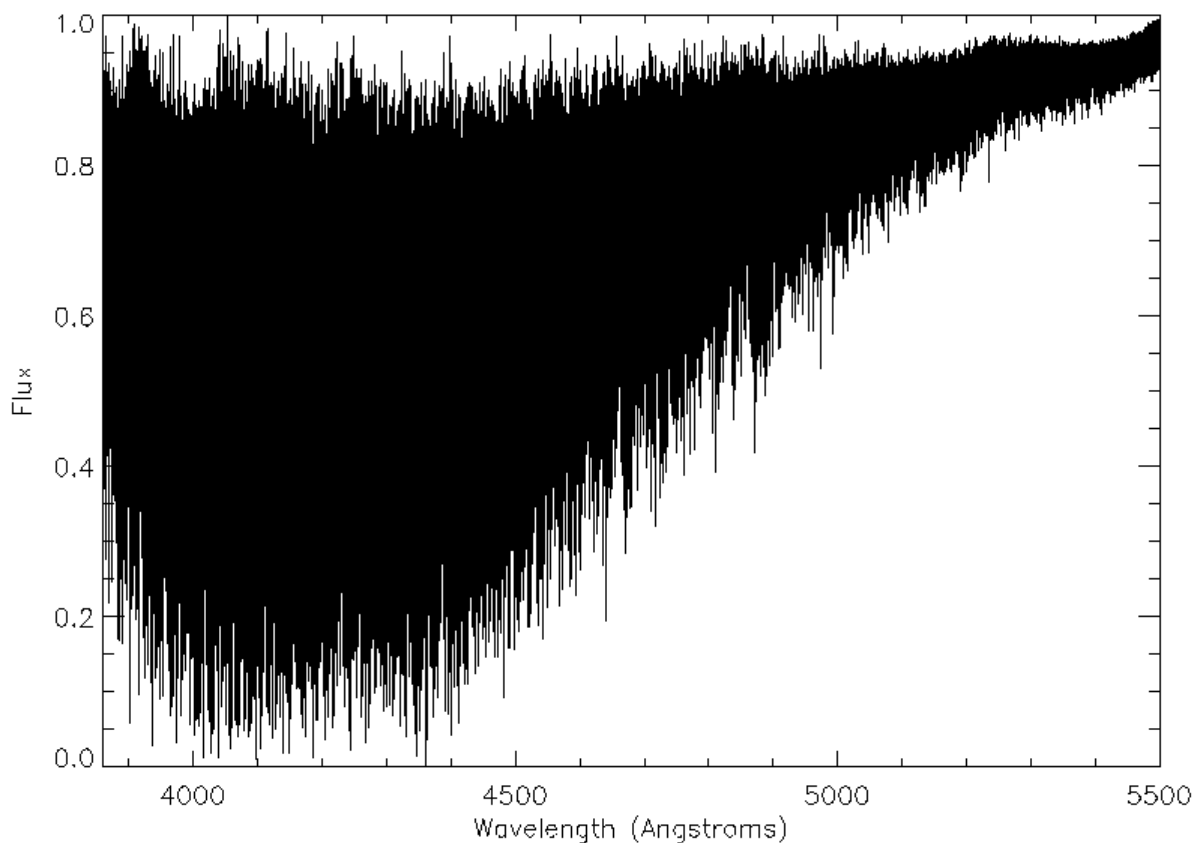
Figure 5.2: The continuum normalized spectrum of the tellurium cell from the fifth run, at a temperature somewhere above the previous figure.

~ 7000 new lines that the tellurium cell makes available for measurements.

The ideal line depth for high precision RV work is $15 - 30\%$ at typical planet hunting resolutions. As can be seen in Fig. 5.4, however, the present cell contains too much tellurium, as the strongest lines have depths of more than 60%. Assuming a linear relation between the pressure and absorption, halving the pressure of the tellurium in the cell will bring the line depths into the ideal range.
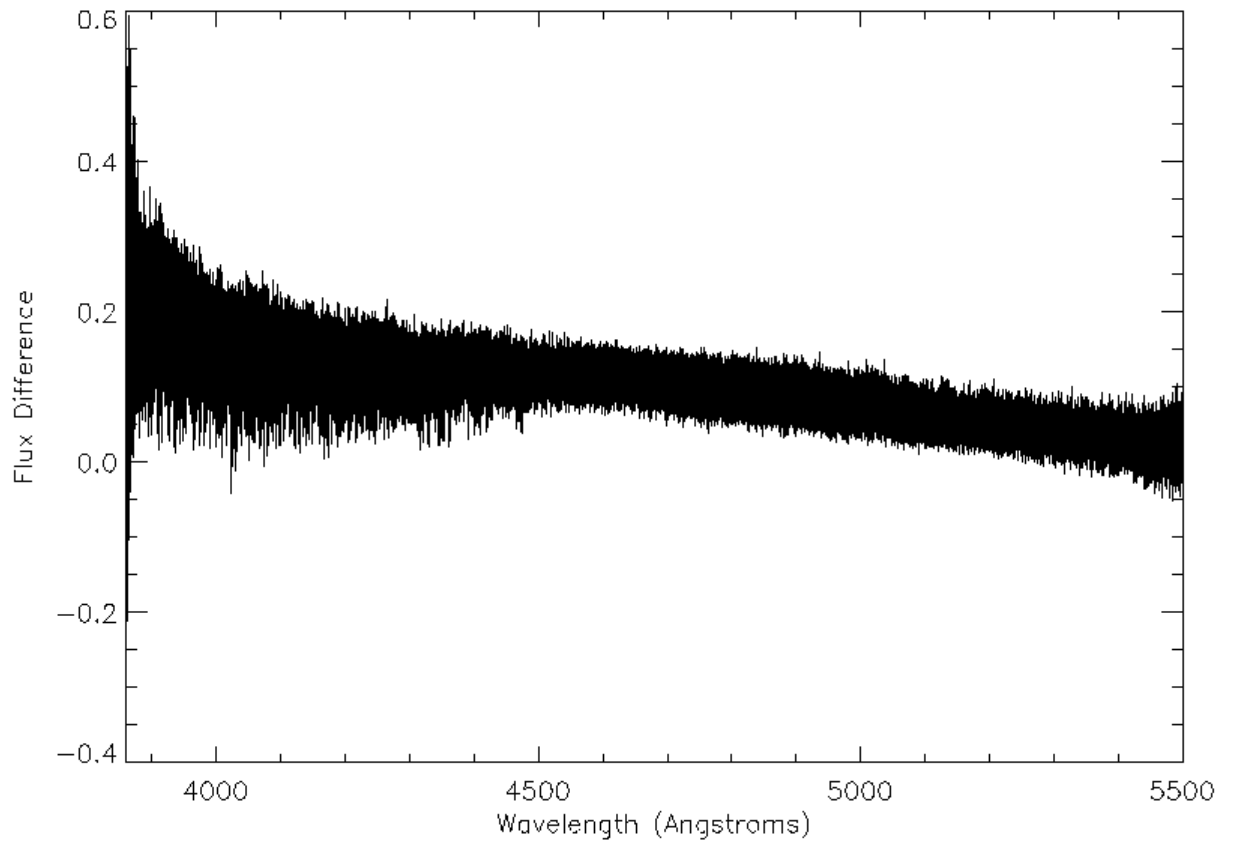
Figure 5.3: The difference in continuum normalized line depth between fourth and fifth runs. The y axis shows the fourth run subtracted from the fifth. A positive difference indicates that the lines in the fifth run are deeper than the fourth, meaning that the tellurium lines deepen as the temperature gets higher.
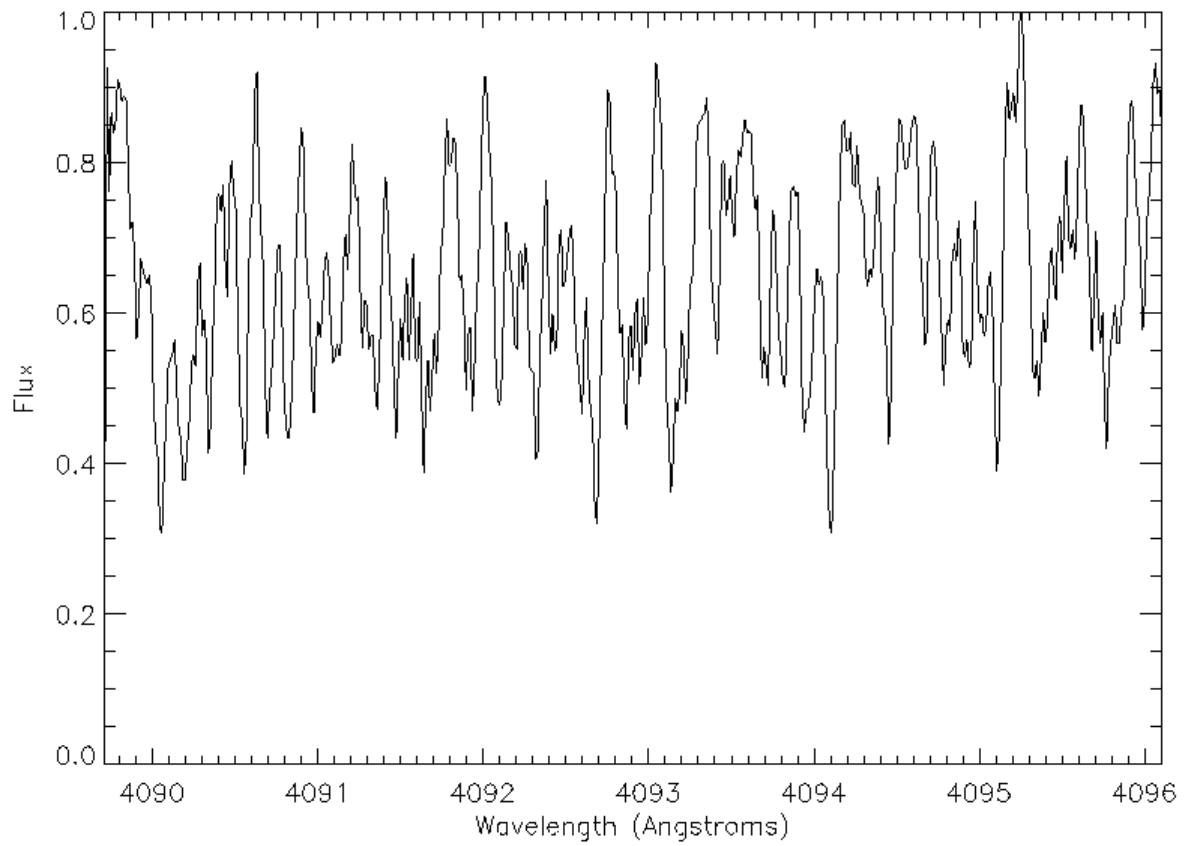
Figure 5.4: The spectrum from Fig. 4.2 run through a boxcar smoother to show what the spectrum would look like at a typical planet-hunting resolution of $\sim 80,000$.

6 Conclusions

The testing of the tellurium cell at NIST was a success, and valuable lessons were learned that can be put into the next iteration of the tellurium cell. The temperature of the cell will need to be tightly controlled to keep the line depths constant over the course of an observing run, and the next version of the cell will need to have a reduced amount of tellurium present. The thermal radiation was kept under control and the remainder could be subtracted away, meaning that the cell functioned very well and has the potential to achieve the initial design goals in the next several phases of testing.

Given the apparent useful wavelength range of the cell of $\sim 3850 - 5000$ Å, it would be best used in tandem with an iodine cell to provide full coverage of the B and V spectral bands, thereby netting many more useful spectral lines on a single exposure, leading to far better precision than has been possible previously with the gas-cell technique. Since the only unwanted radiation escaping the cell is thermal, and that can be blocked by a hot mirror, it would not affect the instrument or the iodine cell in any adverse way. However, due to the overlap between the tellurium and iodine lines, careful modelling would be necessary to separate the two or model the blending of lines that would presumably occur. This could be a difficult problem. Nevertheless, even if it proves to be intractable, the fact that the tellurium cell adds many features blueward of the iodine cell's range, where the spectra of late type dwarf stars have the most features, more than makes up for this potential loss in coverage.

The results presented above show that the tellurium cell is a viable next step in using gas

absorption cells for RV detection that can increase the precision of these measurements. Further testing and investigation, as well as design improvements to the cell assembly itself (most notably the inclusion of hot mirror windows, tight temperature control, and a lower tellurium pressure), will be necessary to ascertain whether it can probe as deeply as hoped, but the chances that it can appear to be very good.

Appendix A Blackbody calculations

The heaters are maintained at 825 K, and have roughly the same surface area as the cell itself, excepting the ends; this means that the outward-directed radiation is coming from the sides of a cylinder with radius 1.25 cm and length 10 cm. Assuming an emissivity ϵ of 0.5, by the Stefan-Boltzmann power law, $P = A\epsilon\sigma T^4$, they radiate approximately 100 W of power that will be absorbed by the dewar.

The ends of the cell also radiate in the visible, and this cannot be blocked by a hot mirror. The total power radiated by the cell windows to the outside of the dewar is

$$P = A\Omega \int \frac{2hc^2}{\lambda^5} \frac{1}{e^{hc/\lambda kT} - 1} d\lambda \tag{A.1}$$

where A is the surface area of the window, Ω is the solid angle subtended by the telescope beam from the point of view of the window, and T the temperature of the cell.

As seen in Fig. 4.4, the cell ends are ~ 1 in. wide, and 1.4 in. away from the outside surface of the dewar window. Assuming the telescope beam is perfectly collimated to the cell's width, and that, as a worst case scenario, the detector were pressed almost right up to the glass, the solid angle would be

$$\Omega = \int_0^\theta \int_0^{2\pi} \sin(\theta')d\theta'd\phi \approx .36 \tag{A.2}$$

as by trigometry $\theta = \tan^{-1}(.5\,\text{in.}/1.4\,\text{in.})$. Using a wavelength range of 300 nm to 1.1 μm as that which we can't block to avoid losing spectral information, the total power emitted by the windows into the beam, assuming a perfect blackbody, is $\sim 5 \times 10^{-4}$ W. Fused silica does not glow strongly in the visible, as can be seen in Fig. 4.3, so its emissivity in the visible must be low even at 825 K,

where the cell will be operated. Assuming an emissivty of ~ 0.001, this further drives down the power emitted into the telescope beam to only $5 \times 10^{-7}\,\mathrm{W}$.

Bibliography

[1] Bouchy, F., Pepe, F. & Queloz, D. 2001, 'Fundamental photon noise limit to radial velocity measurements', *Astronomy & Astrophysics*, vol. 374, pp. 733-739.

[2] Bouchy, F., et al. 2009, 'Charge transfer inefficiency effect for high-precision radial velocity measurements', *EAS Publications Series*, vol. 37, pp. 247-253.

[3] Burns, I. S., Hult, J. & Kaminski, C. F. 2006, 'Use of ^{130}Te$_2$ for frequency referencing and active stabilisation of a violet extended cavity diode laser', *Spectrochemica Acta Part A*, vol. 63, pp. 905-909.

[4] Butler, R. P., et al. 1996, 'Attaining doppler precision of $3\,\mathrm{m\,s^{-1}}$,' *Publications of the Astronomical Society of the Pacific*, vol. 108, pp. 500-509.

[5] Cochran, W. D., et al. 2008, 'Radial velocity planet detection using a gas absorption cell', *Precision Spectroscopy in Astrophysics: Proceedings of the ESO/Lisbon/Aveiro Conference held in Aveiro, Portugal, 11-15 September 2006*, pp. 175-180.

[6] Drummond, D. G. 1936, 'The infra-red absorption spectra of quartz and fused silica from 1 to $7 \cdot 5\,\mu$,' *Proceedigs of the Royal Society of London. Series A, Mathematical and Physical Sciences*, vol. 153, no. 879, pp. 328-339.

[7] Dumusque, X., et al. 2011, 'Planetary detection limits taking into account stellar noise: I.

Observational strategies to reduce stellar oscillation and granulation effects', *Astronomy & Astrophysics*, vol. 525, pp. 140-151.

[8] Dumusque, X., et al. 2011, 'Planetary detection limits taking into account stellar noise: II. Effect of stellar spot groups on radial-velocities', *Astronomy & Astrophysics*, vol. 527, no. A82.

[9] Foot, C. J. 2005, *Atomic Physics*, Oxford University Press, New York, pg. 152.

[10] Griffin, R. & Griffin, R. 1973, 'On the Possibility of determining stellar radial velocities to $0.01\,\mathrm{km\,s^{-1}}$', *Monthly Notices of the Royal Astronomical Society*, vol. 162, pp. 243-253.

[11] Koch, A. & Wöhl, H. 1984, 'The use of molecular iodine absorption lines as wavelength references for solar Doppler shift measurements', *Astronomy & Astrophysics*, vol. 134, pp. 134-138.

[12] Lovis, C., et al. 2006, 'The exoplanet hunter HARPS: unequalled accuracy and perspectives toward $1\,\mathrm{cm\,s^{-1}}$ precision', *Proceedings of the SPIE*, vol. 6269, pp. 62690P-62690P-9.

[13] Lovis, C. & Pepe, F. 2007, 'A new list of thorium and argon spectral lines in the visible,' *Astronomy & Astrophysics*, vol. 468, pp. 1115-1121.

[14] Marcy, G. W. & Butler, R. P. 1992, 'Precision radial velocities with an iodine absorption cell', *Publications of the Astronomical Society of the Pacific*, vol. 104, pp. 270-277.

[15] Mayor, M. & Queloz, D. 1995, 'A Jupiter-mass companion to a solar-type star', *Nature*, vol. 378, pp. 355-359.

[16] Pepe, F. A. & Lovis, C. 2008, 'From HARPS to CODEX: exploring the limits of Doppler measurements', *Physica Scripta*, vol. T130.

[17] Valenti, J., Butler, R. P., & Marcy, G. W. 1995, 'Determining spectrometer instrumental profiles using FTS reference spectra,' *Publications of the Astronomical Society of the Pacific*, vol. 107, pp. 966-976.

[18] Wolszczan, A. & Frail, A. D. 1992, 'A planetary system around the millisecond pulsar PSR1257+12', *Nature*, vol. 355, pp. 145-147.